# Characterization of Activated Charcoal

RIAZ QADEER[1], JAVED HANIF[1], M. SALEEM[2] AND M. AFZAL[2]
*Pakistan Institute of Nuclear Science and Technology,*
*P.O. Box. No. 1356, Islamabad, Pakistan*
*[2]Department of Chemistry, Quaid-i-Azam University,*
*Islamabad, Pakistan*

(Received December 4, 1993, revised April 11, 1994)

**Summary:** The structural investigations of a commercial activated charcoal were carried out using different techniques such as X-ray diffraction, thermal analysis, nitrogen adsorption and mercury porosimetry. X-ray diffraction study revealed that the activated charcoal is amorphous in nature and has micro-crystalline structure. The thermogravimetric study of activated charcoal showed that the weight loss occurred in two distinct regions: one endothermic (dehydration) and other exothermic (combustion). The moisture and ash contents were found to be 11% and 10% respectively. The pore size distribution curve and D-R analysis of nitrogen adsorption isotherm indicates the microporous nature of the activated charcoal with surface area 1000 $m^2/g$, porosity 75.74% and pore volume 1.43 $cm^3/g$

## Introduction

Activated charcoals are porous materials which are extensively used as adsorbents, catalysts and catalyst supports [1-4]. The purification of gases and the recovery of the solvent represent some of their most frequent applications. Besides these, the activated charcoals have found many applications to remove the toxic and health hazardous particles and ions from industrial effluents [5-7]. The activity of activated charcoal is based on its physical adsorption capacity which itself depends on the porosity and the surface properties of the adsorbent. The chemical nature of the activated charcoals is associated with the intrinsic properties of the parent materials and with the manufacturing and activation methods. The present work is carried out to characterize a commercial activated charcoal (BDH, item No. 33032) using different techniques such as X-ray diffraction, thermal analysis, nitrogen adsorption and mercury porosimetry.

## Results and Discussion

### *X-ray diffraction study*

The X-ray diffractogram of activated charcoal, shown in Figure 1, has a diffused halo with peak maximum at 2θ values equaling 22, points towards the amorphous nature of the activated charcoal. A glimpse of the microstructure of the activated charcoal is observed from the calculation of mean crystallite size or mean defect distance (LC) using the Scherrer equation using method of Short and Walker [9].

$$LC = \frac{57.3\ K\lambda}{\beta Cos\theta} \qquad (1)$$

where K is the Scherrer constant, λ is the wavelength of X- radiation, β is the peak width in degree (2θ) at

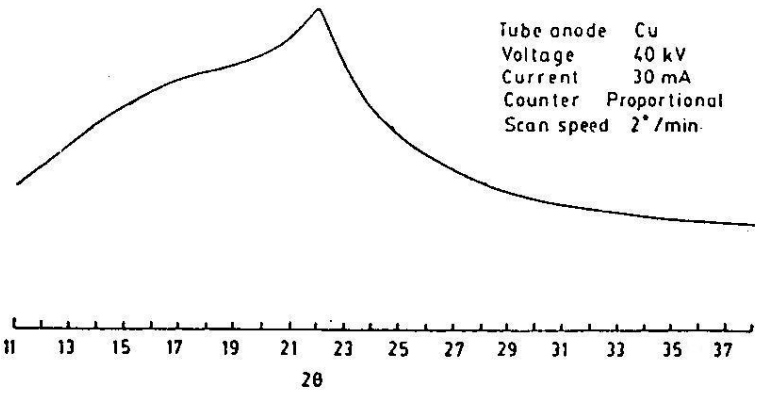


Fig. 1: X-ray diffraction pattern of activated charcoal.

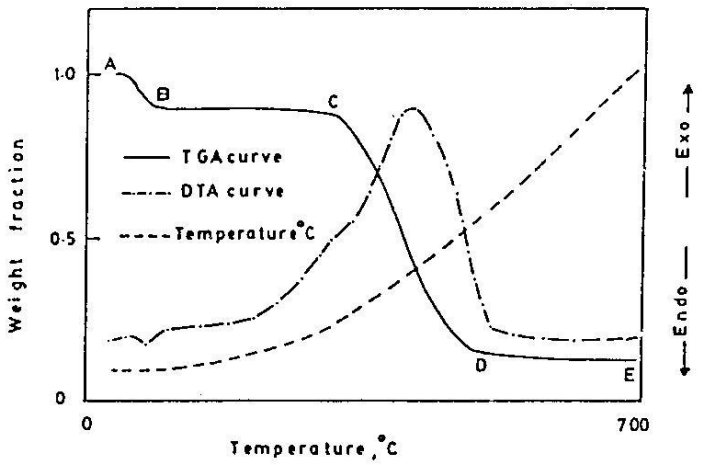


Fig. 2: TG/DTA curves for activated charcoal.

half width. The LC value for activated charcoal is 3.98 nm. This higher value of the LC obviates the somewhat ordered nature of the carbon layers, thus decreasing the degree of amorphousness. The relatively narrow peak (halo) is supportive of the above argument.

*Thermal analysis of activated charcoal*

Figure 2 shows TG/DTA curves for activated charcoal, the inspection of which shows that the weight loss occurs in two distinct steps; one endothermic and the other largely exothermic. In the first step, from A-B (25 - 117°C) the weight loss occurs due to dehydration. The dehydration step terminates at about 117°C with a weight loss of 11%. From B-C, there is a thermally stable region in the temperature range of 117 to 390°C. From C-D, major weight loss occurs which is due to the combustion of charcoal in the temperature range from 390 to 700°C. It is a matter of common observation that the oxidation of carbon occurs below 600°C [10]. The total weight loss from point A to D was about 90% and remaining 10% is the ash content.

The activation energies for the dehydration and combustion processes for activated charcoal were calculated using the relation proposed by Horwitz and Metzger [11] as

$$\ln \ln \frac{W_o - W_f}{W - W_f} = \frac{E\theta}{RT_s^2} \qquad (2)$$

where W is the weight at a given temperature, $W_o$ and $W_f$ are the initial and final weights respectively, $T_s$ is the temperature where $(W-W_f)/(W_o-W_f) = 1/e$ and $\theta = (T-Ts)$. The plots of ln ln $[(W_o-W_f)/(W-W_f)]$ versus $\theta$ yield straight lines, Figure 5, with slope equal to $E/RT_s^2$. From the slopes of these lines the values of activation energies for the dehydration and combustion processes were calculated as 52.89 and 94.20 kJ/mol respectively, which are in good agreement to the values observed by other workers [12].

*Nitrogen adsorption*

The nitrogen adsorption and desorption isotherms are shown in Figure 3 where amount of nitrogen adsorbed and desorbed are plotted against the relative pressure $P/P^o$. Such isotherms are not typical for the activated charcoal due to an abrupt increase in the amount adsorbed/desorbed for relative pressure > 0.75. These isotherms may be classified as a mixture of I and II type [13-14]. Such behavior is a characteristic of penetration in micropores, followed by a monolayer-multilayer adsorption and interparticle capillary condensation [15].

Thespecific surface area of the activated charcoal was determined by applying the B.E.T. equation to the physical adsorption data of nitrogen at 77 K. The most convenient form of B.E.T. equation for the application to experimental data is given below [16].

$$\frac{1}{X[P^o/p)-1]} = \frac{1}{X_mC} + \frac{C-1}{X_mC}\,\frac{P}{P^o} \qquad (3)$$

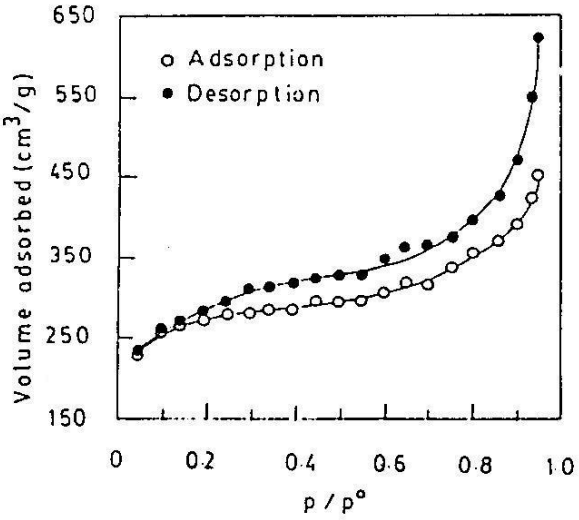


Fig. 3: Nitrogen adsorption-desorption isotherms at 77K on activated charcoal.

on activated charcoal is shown in Figure 6. From the slope ($C-1/X_mC$) and intercept ($1/X_mC$), the values of $X_m$ and C were calculated and are $4.97 \times 10^{-3}$ and 167.66 respectively. From the value of mono-layer capacity ($X_m$), the surface area was calculated using the known molecular cross section of the nitrogen molecule (16.2 Å at 77 K) which comes out to be 1000 $m^2/g$.

B.E.T. plot, Figure 6, shows that experimental points deviate from linearity with the increase in the relative pressure. This deviation from linearity is apparent at the relative pressure greater than 0.25. It has been shown by Brunauer [17] that for $P/P^o$ value greater than 0.30, the experimental points do not fall on a straight line. In other words, the B.E.T. equation breaks down for the less active points on the surface. At relative pressures above 0.3, the experimental points of B.E.T. equation deviate strongly from linearity. Herman and Emmett [18], indicated that B.E.T. equation gives reasonable values in the range of relative pressure from 0.05 to 0.35. They concluded that in this range of relative pressure, monolayer is formed and B.E.T. C values usually gives heat of adsorption. Thus in the relative

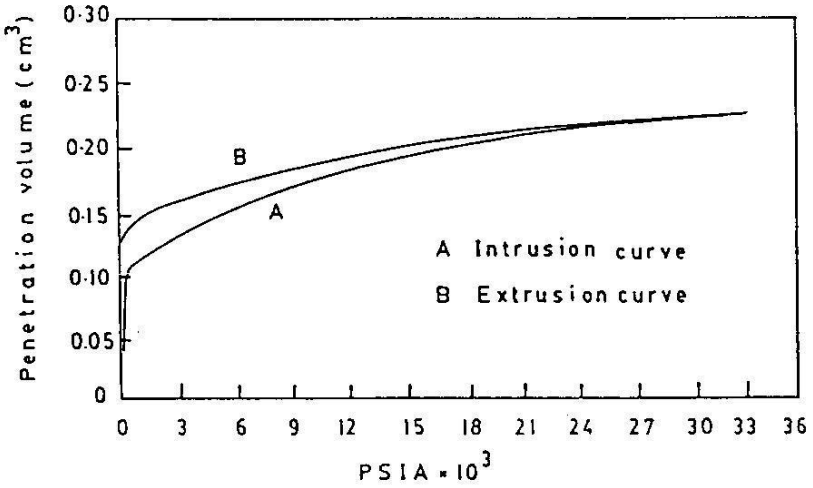


Fig. 4: Mercury intrusion and extrusion curves for activated charcoal.

where all the symbols have their usual meanings. The B.E.T. equation (3) gives a linear relationship between $1/X\ [(P^o/P-)1]$ and $P/P^o$. The range of linearity is usually restricted to a limited part of the isotherm. B.E.T. plot for the adsorption of nitrogen

pressure range 0.05 to 0.35, the linear B.E.T. range apparently represents a condition in which the very high energy sites have been occupied and extensive multilayer adsorption has not yet commenced. It is within these limits that the B.E.T. equation is

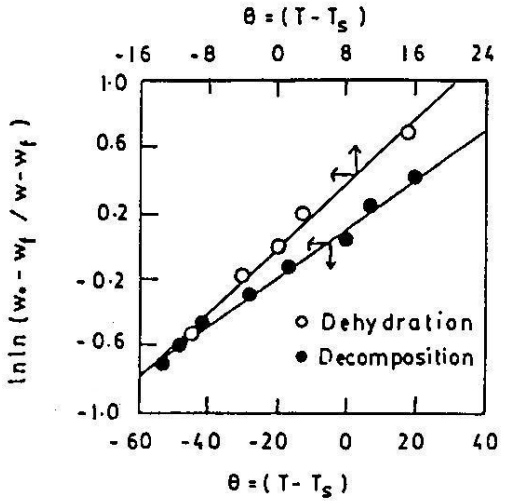


Fig. 5: Plots of ln ln $[(W_o-W_f)/(W-W_f)]$ against for activated charcoal.

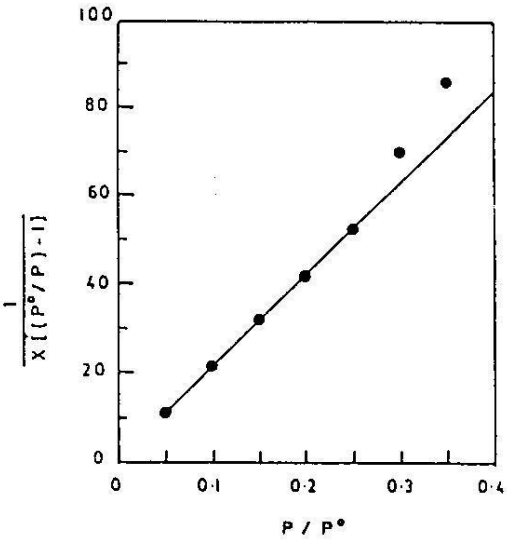


Fig. 6: B.E.T. plot for activated charcoal.

generally valid and deviations from this range of linearity reflect unusual surface properties. In microporous substances, the narrow pores exhibit high energy potentials due to overlapping potential from the walls of the micropores. Under these conditions condensation can occur within the pores at relative pressure less than 0.35 and linear B.E.T. plot is found at even lower relative pressure [19].

The pore volume measured by nitrogen adsorption is 0.88 $cm^3/g$. The pore size distribution of activated charcoal, shown in Figure 7, is

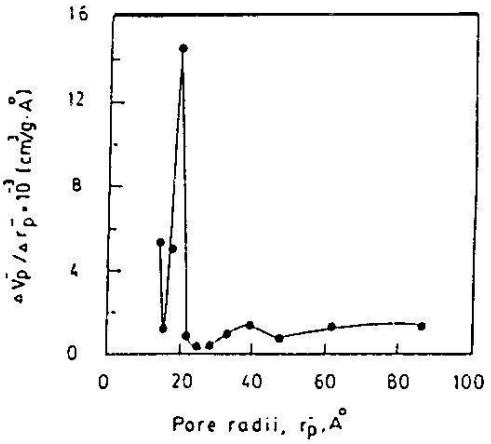


Fig. 7: Pore size distribution curve for activated charcoal.

calculated by applying the Kelvin equation [20]. This distribution indicates one sharp peak at pore radius ~19 Å and other small and broad peak at pore radius ~40 Å. This shows the microporous character of the activated charcoal with some mesopores. The major contribution to total pore volume comes predominately from micropore of radius ~ 19Å. The distribution was cut off on lower end at 15, since the Kelvin equation is considered valid for pores radius no smaller than 15Å [21]. No correct theory is ~capable of providing a general description of micropore filling. The fact is that a particular equation gives a reasonably good fit over a certain range of an isotherm does necessarily provide sufficient evidence for a particular mechanism of adsorption to be operative. Adsorption by a microporous solid in general and by activated charcoal in particular, is described by the Dubinin's theory for the filling of micropores and its subsequent developments [22-23]. The Dubinin-Raduskevich (DR) equation in its usual form has been used to calculate the volume of the micropore [24].

$$V = V_0 \exp - B(T/\beta)^2 \log^2(P^o/P) \qquad (4)$$

where V represents the volume of the adsorbate at temperature T and at relative pressure $P/P^o$ and $V_o$ is the total volume of micropores. B and β are specific constants depending respectively on the nature of the solid and on the adsorptive. To obtain the micropore volume from $V_o$, the adsorbate is assumed to be liquid like [25]. The DR plot for activated charcoal is shown in Figure 8, which is obtained by plotting log

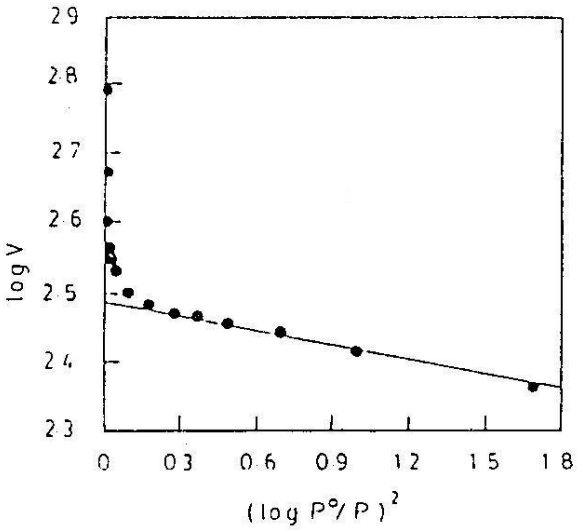


Fig. 8: D-R plot of nitrogen adsorption at 77K on activated charcoal.

V verses $\log^2 (P^O/P)$ according to equation 4. This plot exhibits a straight line at lower relative pressures and apparent upward deviation at higher relative pressures. The deviation from straight line shows that activated charcoal has heterogeneous system of micropores [26]. The experimental points at relatively lower pressures are selected to obtain the $V_o$ values. The straight line is extrapolated to $\log^2(P^O/P) = O$ and from the intercept, the $V_o$ (micropore) volume was calculated as (0.46 $cm^3/g$). This shows that microporosity is highly developed in the activated charcoal. The value of $V_o$ is very close to the micropore volume deduced directly from the adsorption isotherms at $P/P^o = 0.20$.

*Mercury porosimetry*

The plot of intrusion and extrusion volume as function of applied pressure for activated charcoal are given in Figure 4. This shows that there is a steep initial portion in the intrusion plot which gradually goes flat at higher pressure. The high initial slope of the intrusion plot is attributed to intrusion into the large pores and interstices between particles [19]. Once the mercury has gained entry into the large pore and inter particulate spaces, the intrusion occurs into progressively smaller pores as the pressure is raised. Above 27000 PSIA pressure, no appreciable intrusion takes place indicating that little pore volume exists in the pores of radii smaller than 0.0040 micrometers. The extrusion curve shows that mercury extrusion do not follow the same path. This intrusion extrusion hysteresis can be explained by a change in contact angle of mercury between intrusion and extrusion. This irreversi- bility indicates that the pores of activated charcoal are not cylindrical in nature [27]. According to Dubinin *et al.* [28], the irreversibility of the hysteresis shows the evidence of "Ink-bottle" pores. Another factor contributing to hysteresis is the influence of the pore potential which can act to trap mercury once it intrudes into the pores. The pore size distribution as determined from mercury penetration is given in Figure 9, which shows a peak at pore radius 40 Å. This indicates the contribution of pores having radius 40 Å to the total pore volume. A small peak at 40 Å was also observed in the pore size distribution curve in the nitrogen adsorption as shown in Figure 7. The values of pore volume (1.43 $cm^3/g$) measured by mercury porosimeter is greater than those estimated from nitrogen adsorption (0.88 $cm^3/g$). This observation may be explained by (i) sample compression at higher pressures of mercury causing unrealistically higher values of pore volume [29], (ii) nitrogen adsorption study provides data only in the mesopores and micropore region, while mercury intrusion also includes pore volume data for macropore [21].

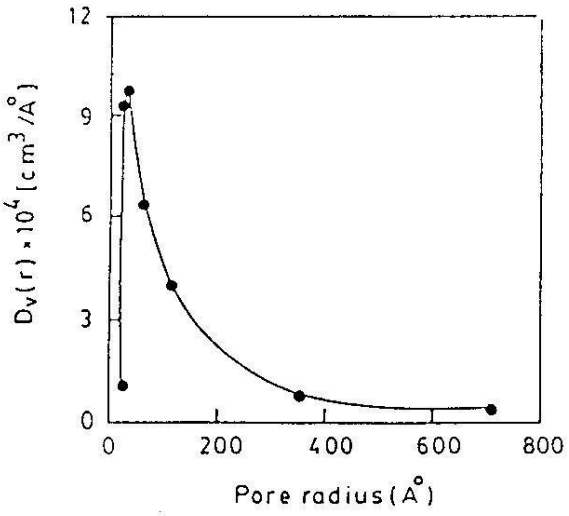


Fig. 9: Pore size distribution curve for activated charcoal determined from mercury penetration.

The surface area value of the activated charcoal determined by means of mercury intrusion is 166 $m^2/g$, which does not agree with the surface

area found from nitrogen adsorption. Small surface area by mercury porosimetry indicates the presence of a microporous system which is only accessible to nitrogen molecules. High value of surface area by nitrogen adsorption is totally attributable to microporosity of activated charcoal which can be determined by mercury porosimeter.

## Experimental

*X-ray diffraction study*

Diffraction pattern of the activated charcoal was obtained with a Phillips PW 1060/70 diffractometer. The detector was an argon filled proportional counter linked to a PW 1390 rate meter and channel analyzer. The radiation was Cu $K_\alpha$ (1.5418Å) generated in a Phillips PW 1730 generator operated at 40kV and 20 mA. Diffraction pattern obtained for activated charcoal is shown in Figure 1.

*Thermal analysis of activated charcoal*

Thermal study of the activated charcoal was carried out using simultaneous thermal analyzer, STA-784 from M/S Stanton Red Croff, England. A known amount of activated charcoal was taken in a crucible and its dehydration and combustion was carried out from room temperature to 700°C, at a ramping rate of 20°C/min. The experiment was performed in static air. The TG/DTA curves are shown in Figure 2.

*Nitrogen adsorption*

Surface area and pore size distribution of the activated charcoal were measured using the Quantasorb Sorption system (M/S Quantachrome Corporation, N.Y.) by continuous flow method [8]. The process of adsorption and desorption are monitored by measuring the change in the thermal conductivity of the gas mixture. The thermal conductivity of the gas mixture was monitored differentially by thermal conductivity cell placed before and after the sample cell. A mixture of nitrogen (adsorbate) and helium (carrier) of known concentration was passed over a sample which was previously outgassed at 110°C by heating. The adsorption was started by immersing the sample cell containing known amount of activated charcoal in a liquid nitrogen coolant. The adsorption peak was produced by the change in the thermal conductivity of the gas mixture resulting from a decrease in nitrogen concentration due to adsorption on sample surface. The adsorption was completed, until there was no difference in the thermal conductivities of gas entering or leaving the sample cell. The adsorbed nitrogen was then desorbed by removing the coolant and the liberated nitrogen was monitored by thermal conductivity detector. The volume of adsorbed nitrogen was calculated. The same measurements were carried out at different $He/N_2$ ratio obtained by adjusting the gas flow rates and data points were obtained to construct the entire adsorption/desorption isotherm, shown in Figure 3.

*Mercury porosimetry*

The porosity, pore volume and surface area of the activated charcoal were measured by Autoscan-33 Mercury Porosimeter (M/S Quanta- chrome Corporation, U.S.A.). The mercury was intruded into pores of activated charcoal as a function of pressure. The mercury intrusion curve for activated charcoal is given in Figure 4. The data was corrected for compression of mercury by taking blank measurement with mercury.

## References

1. Y. Suda, T. Morimoto and M. Nagao, *Langmuir*, **3**, 99 (1987).
2. D.M. Ruthven, N.S. Raghavan and M.M. Hassan, *Chem. Eng. Sci.*, **41**, 1325 (1986).
3. J.E. Koresh and A. Sofer, *Sep. Sci. Technol.*, **18**, 723 (1983).
4. G.C. Brunewald and R.S. Drago, *J. Mol. Catal.*, **58**, 227 (1990).
5. D.W. Underhill, *Nucl. Sci. Engg.*, **79**, 19 (1981).
6. T. Yamamoto, K. Tsukui and N. Ootsuka, J. Nucl. Sci. Technol., **21**, 372 (1984).
7. T.P. Vo and T. Frot, Jr., *J. Phys. Chem.*, **91**, 6638 (1987).
8. F.M. Nelsen and F.T. Eggertsen, *Anal. Chem.*, **30**, 1387 (1958).
9. M.A. Short and P.L. Walker Jr., Carbon, **1**, 3 (1963).
10. P.P. Kozakevich and N.A. Izmailov, *Kollaid Z.*, **57**, 294 (1929).
11. H.H. Horowitz and B. Metzger, *Anal. Chem.*, **35**, 1464 (1963).
12. P. Gonzalez-Vilchez, A. Linares-Solano, J. De. D. Lopez-Bonzalez and F. Radriguez-Reinoso, *Carbon*, **17**, 441 (1979).
13. J.M. Martin-Martinez, M. Molina-Sabio, F. Rodriguez-Reinoso and R. Torregrosa, *Fuel*, **68**, 204 (1989).

14. M.J. Selles-Perez and J.M. Martin-Martinez, *J. Chem. Soc. Faraday Trans.I*, **87**, 1237 (1991).
15. M.M. Dubinin, *J. Colloid Interface Sci.*, **23**, 487 (1967).
16. S. Lowell, Introduction to Powder Surface Area, John Willey & Sons, N.Y. P.25 (1979).
17. S. Brunauer, Solid Surfaces and the Gas Solid Interface, Advances in Chemistry Series No. 33, American Chemical Society, Washington D.C. (1961).
18. R.G. Herman and P.H. Emmett, Catalysis, Fundamental Principles (Part I) Vol. 1, Ed. P.H. Emmett, Reinhold Pub. Corp., N.Y. (1954).
19. S.J. Gregg and K.S.W. Sing, Adsorption, Surface area and Porosity, Academic, New York (1967).
20. C.H. Giles, D.C. Havard, W. McMillan, T. Smith and R. Wilson, In Characterization of Porous Solids (Proceedings of a Symposium held at Universite de Neuchatel, Switzerland from 9-12 July, (1978). Eds. S.J. Gregg, K.S.W. Sing and H.F. Stoeckli, London, Society of Chemical Industry, 267-284 (1979).
21. W.E. White, C.H. Bartholomew, W.C. Hecker and D.M. Smith, *Ads. Sci. Technol.*, **7**, 180 (1990).
22. M.M. Dubinin, In Progress in Surface and Membrane Science Vol. 9, Ed. D.A. Cadenhead, Academic Press, New York P. 1-70 (1975).
23. H.F. Stoeckli, J. Ph. Houriet, A. Parret and U. Huber, In Characterisation of Porous Solids (Proceedings of a symposium held at Universite de Neuchatel, Switzerland from 9-12 July, 1978) Eds. S.J. Gregg, K.S.W. Sing and H.F. Stoeckli, London: Society of Chemical Industry P. 31 (1979).
24. M.M. Dubinin, *J. Colloid Interface Sci.*, **75**, 39 (1980).
25. T.S. Lamond and H. Marsh, *Carbon*, **1**, 293 (1964).
26. F. Stoeckli and J.P. Houriet, *J. Colloid Interface Sci.*, **62**, 195 (1978).
27. P.H. Emmett, *Chem. Rev.*, **43**, 69 (1948).
28. M.M. Dubinin, M.M. Vishnyakova, E.A. Leontev, V.M. Lukyanovich and A.I. Sarachov, *Zhur. Fiz. Khim.*, **34**, 2019 (1960).
29. C.L. Glaves, P.J. Davis, D.P. Gallegos and D.M. Smith, *Energy Fuels*, **22**, 662 (1988).